Figures of Merit for Color Scanners

Gaurav Sharma, *Member, IEEE,* and H. Joel Trussell, *Fellow, IEEE*

***Abstract*—In the design and evaluation of color scanners and cameras, it is useful to have a single figure of merit that closely agrees with perceived color accuracy. In the past, several measures of goodness for color scanning filters have been proposed to fulfill such a requirement. Most of the proposed measures have had shortcomings in that they are either based on error metrics in color spaces that are not perceptually uniform, or in that they do not take into account the effects of measurement noise. In this paper, an extension of the most promising measure, based on linearized CIELAB space, is proposed to obtain a new figure of merit that has a high degree of perceptual relevance and also accounts for the varying noise performance of different filters. The paper also provides a common framework for the different figures of merit and a comprehensive comparison of their computational complexity and reliability.**

I. Introduction

THE perception of color involves interaction between a physical stimulus (light) and the human visual system. Hence, color differs fundamentally from other physical quantities in that its specification and measurement must perforce take into account the characteristics of the observer. The CIE has defined color-matching functions for a standard colorimetric observer and uniform color spaces [1], [2] that capture properties of the human visual system relevant to colorimetry. These standards provide a consistent definition of color necessary for colorimetry and for the meaningful exchange of color information.

Color scanners and cameras that strive for colorimetric reproduction must also take into account the properties of the human visual system in their design and in the interpretation of data obtained from physical sensors. Measurement noise and practical limitations in fabricating these systems often limit the color accuracy of these devices. A figure of merit for color scanners and cameras that relates closely to color accuracy is therefore desirable for their evaluation and design.

A "quality factor" for color filters was first proposed by Neugebauer [3]. Neugebauer's quality factor was, however, limited to the evaluation of single filters. Vora and Trussell [4] extended the quality factor to filter sets with an arbitrary number of filters. An alternate measure, called the color quality factor (CQF) [5], has also been used in the industry for the evaluation of filter sets with multiple filters.

Manuscript received April 5, 1996; revised January 28, 1997. The associate editor coordinating the review of this manuscript and approving it for publication was Dr. Ping Wah Wong.

G. Sharma is with Xerox Corporation, Webster, NY 14580 USA (e-mail: sharma@wrc.xerox.com).

H. J. Trussell is with the Electrical and Computer Engineering Department, North Carolina State University, Raleigh, NC 27695-7911 USA (e-mail: hjt@eos.ncsu.edu).

Publisher Item Identifier S 1057-7149(97)04732-5.

The aforementioned measures can all be related to a mean squared error (MSE) metric in CIE XYZ space. Since the CIE XYZ space is known to be perceptually extremely nonuniform, a measure based on a uniform color space, such as the CIELAB space [1], [2], could offer significant advantages over these measures. Such a measure was implicit in the formulation used by Vrhel and Trussell [6] for the design of filters. The nonlinear nature of uniform color spaces, however, necessitates a considerable increase in computation. Recently, Wolski *et al.* [7], [8] proposed the use of global and local linearizations of CIELAB space to reduce the computational complexity while preserving the desirable property of perceptual uniformity.

All the measures described so far are formulated with the assumption that the scanner/camera sensors are noiseless. In the real world, sensor noise is inevitable. Since filter sets need not be equally robust in the presence of measurement noise, a single figure of merit combining the filters and the information of noise statistics is more desirable. Vrhel and Trussell [9], [10] accounted for sensor noise in the design of color scanning filters. However, the work was based on a mean squared error metric in the perceptually nonuniform CIE XYZ space.

In this paper, a new figure of merit for color scanners/cameras is considered that can be viewed as extension of the work in [7], [8], and [10]. The new figure of merit is based on an error metric in linearized CIELAB space and incorporates a model for measurement noise. It therefore has a high degree of perceptual relevance and also accounts for the noise performance of different filters. This claim is validated by the simulation results presented in Section VII. This work also provides a comprehensive comparison of the reliability and computational complexity of the different figures of merit in a unified framework.

For notational convenience and brevity, the subsequent discussion in this paper will refer to a color scanner scanning images on reflective media. However, with trivial modifications the same analysis applies to color cameras and other color measuring devices.

The rest of the paper is organized as follows. Section II introduces the relevant notation for colorimetry and a model for scanner operation. A general error metric for scanners is developed in Section III. Based on this metric, a normalized figure of merit is defined in Section IV and several specific figures of merit are shown to conform to the general framework developed. Section V presents an overview of the different figures of merit, summarizing their similarities and differences, and Section VI describes their computational requirements. Simulation results comparing the reliability of different figures of merit are presented in Section VII and concluding remarks in Section VIII. Some of the mathematical expressions omitted

from the main text of the paper are summarized in the Appendixes.

II. Scanner Colorimetry

The color of an object is specified by its CIE XYZ tristimulus values

$$t_i = \int_{-\infty}^{\infty} a_i(\lambda) l(\lambda) r(\lambda)\, d\lambda, \quad i = 1,2,3 \tag{1}$$

where $\{a_i(\lambda)\}_{i=1}^{3}$ are the CIE XYZ color matching functions [1], [2], $l(\lambda)$ is the spectral radiance of the viewing illuminant, and $r(\lambda)$ is the spectral reflectance of the object.

For computation, the integral in (1) is approximated by a summation involving the corresponding sampled quantities. If N equispaced samples over the visible range are used, the three equations can be written compactly as

$$\mathbf{t}(\mathbf{r}) = \mathbf{A}^T\mathbf{L}\mathbf{r} = \mathbf{A}_L^T\mathbf{r} \tag{2}$$

where $\mathbf{t}(\mathbf{r})$ is the 3×1 vector of CIE XYZ tristimulus values, $\mathbf{A}$ is the $N\times 3$ matrix of CIE XYZ color matching functions, $\mathbf{L}$ is the $N \times N$ diagonal matrix with samples of the illuminant spectrum along the diagonal, $\mathbf{r}$ is the $N \times 1$ vector of the object reflectance, and $\mathbf{A}_L = \mathbf{L}\mathbf{A}$.

Scanner measurements of the object with a K channel scanner can be similarly expressed as

$$\mathbf{t}_s(\mathbf{r}) = \mathbf{M}^T\mathbf{L}_s\mathbf{r} + \boldsymbol{\eta} = \mathbf{G}^T\mathbf{r} + \boldsymbol{\eta} \tag{3}$$

where $\mathbf{t}_s(\mathbf{r})$ is a $K\times 1$ vector of scanner measurements, $\mathbf{M}$ is the $N \times K$ matrix of scanner filter transmittances (including detector sensitivity and the transmittance of the scanner optical path), $\mathbf{L}_s$ is the $N \times N$ diagonal matrix with samples of the scanning illuminant spectrum along the diagonal, $\boldsymbol{\eta}$ is the $K\times 1$ measurement noise vector, and $\mathbf{G} = \mathbf{L}_s\mathbf{M}$.

To obtain colorimetric information from the scanner, the CIE XYZ tristimulus values must be estimated from the scanner measurements. If there is no measurement noise and the product of the viewing illuminant and the CIE XYZ color matching functions can be expressed as a linear combination of the scanner sensitivity curves, then the CIE XYZ tristimulus values are obtained as a linear transformation of the scanner measurements. Mathematically, if $\mathbf{A}_L = \mathbf{G}\mathbf{B}_0^T$, for some matrix $\mathbf{B}_0$ and $\boldsymbol{\eta} = \mathbf{0}$, then $\mathbf{t}(\mathbf{r}) = \mathbf{B}_0\mathbf{t}_s(\mathbf{r})$. For the more practical case, when the sensor responses do not match up to CIE and the measurements are corrupted by noise, the CIE XYZ tristimulus values may still be estimated as linear transformations of the scanner measurements

$$\hat{\mathbf{t}}(\mathbf{r}) = \mathbf{B}\mathbf{t}_s(\mathbf{r}) \tag{4}$$

where the transformation $\mathbf{B}$ is determined so as to minimize the color error.

In addition to linear transformations, polynomial transformations and look-up tables have been used for scanner calibration [11]–[14]. Haneishi *et al.* [12] demonstrated that when calibrating for multiple materials the higher order polynomials offered no advantages over a linear transformation. The same is true of look-up tables (LUT's) [15]. Since the goal of colorimetric scanning is to obtain a material independent calibration, polynomial transformations and LUT's are not considered here.

The color error may be defined in several different ways and accordingly, there will be different "optimal" transformations. The next section elaborates further on the choice of color error metrics and of the transformation, $\mathbf{B}$, in the above equation.

III. A General Scanner Error Metric

The average magnitude of "color difference" between the true color $\mathbf{t}(\mathbf{r})$ and the estimate $\hat{\mathbf{t}}(\mathbf{r})$ may be used as an error metric for quantifying the scanner performance. Different color spaces may be used in the computation of the "color difference." To encompass several cases in a unified treatment, it will be assumed that the error magnitude can be expressed mathematically in the form $\|\mathcal{F}(\mathbf{t}(\mathbf{r})) - \mathcal{F}(\hat{\mathbf{t}}(\mathbf{r}))\|$ where $\mathcal{F}()$ is a 3×3 (possibly nonlinear) transformation of the tristimulus values, and $\|\cdot\|$ denotes the Euclidean vector norm [16]. Such a metric is motivated by the numerous uniform color spaces in which equal Euclidean distances correspond to approximately equal perceptual color errors [2]. In such a scenario, $\mathcal{F}()$ represents the transformation from the CIE XYZ space into a uniform color space.

In terms of the above notation, the scanners mean squared color error is given by

$$\epsilon(\mathbf{A}_L, \mathbf{G}, \mathbf{B}) = E\{\|\mathcal{F}(\mathbf{t}(\mathbf{r})) - \mathcal{F}(\hat{\mathbf{t}}(\mathbf{r}))\|^2\} \tag{5}$$

where $E\{\}$ denotes the expectation over the ensemble of objects to be scanned. As an alternative to the mean squared value, the maximum error over the ensemble, or a variety of other means may be used in the above expression. The mean squared value, however, has the advantage that it preserves differentiability, which is desirable in design applications making use of gradient based methods.

The above error metric quantifies the performance of a scanner "specified by" $\mathbf{G}$ when the transformation $\mathbf{B}$ is used in (4). An error metric for the scanner alone can be obtained by replacing the generic transformation, $\mathbf{B}$, with the optimal transformation that minimizes the error. However, such an error metric is not readily computable, since the optimal transformation cannot be determined in closed form for a general nonlinear transformation, $\mathcal{F}()$. If the transformation $\mathcal{F}()$ is differentiable, with continuous first partial derivatives, a first-order Taylor series provides a fairly accurate locally linear approximation for $\mathcal{F}()$. If $\|\mathbf{t}(\mathbf{r}) - \hat{\mathbf{t}}(\mathbf{r})\|$ is small over the scanned ensemble, this first-order Taylor series can be used to approximate the error metric in (5) by the expected mean-squared linearized color error

$$\begin{aligned}\epsilon(\mathbf{A}_L, \mathbf{G}, \mathbf{B}) &\approx \epsilon_l(\mathbf{A}_L, \mathbf{G}, \mathbf{B}) \\ &= E\{\|J_{\mathcal{F}}(\mathbf{t}(\mathbf{r}))(\mathbf{t}(\mathbf{r}) - \hat{\mathbf{t}}(\mathbf{r}))\|^2\}\end{aligned} \tag{6}$$

where $J_{\mathcal{F}}(\mathbf{t}(\mathbf{r}))$ denotes the Jacobian matrix [17] of the transformation $\mathcal{F}()$ at $\mathbf{t}(\mathbf{r})$. In the subsequent sections, the color space transformation $\mathcal{F}()$ will often be a linear transformation. In such a case, the above approximation is exact and $J_{\mathcal{F}}(\mathbf{t}(\mathbf{r}))$ is the same as $\mathbf{F}$, the matrix representing the linear transformation $\mathcal{F}()$. The transformation that minimizes

the linearized error metric, viz.,

$$\mathbf{B}_{\text{opt}}(\mathbf{A}_L, \mathbf{G}) = \arg\min_{\mathbf{B}} \epsilon_l(\mathbf{A}_L, \mathbf{G}, \mathbf{B}) \tag{7}$$

can then be used to obtain an error metric for the scanner as $\xi(\mathbf{A}_L, \mathbf{G}) = \epsilon_l(\mathbf{A}_L, \mathbf{G}, \mathbf{B}_{\text{opt}}(\mathbf{A}_L, \mathbf{G}))$. As will be illustrated below, the advantage of using the linearized error metric is that closed-form expressions can be obtained for the optimal transformation and for the scanner error metric.

If the measurement noise, $\boldsymbol{\eta}$, is zero mean and independent of $\mathbf{r}$, then it can be seen that the optimal transformation in (7) is given by

$$\begin{aligned}\text{vec}(\mathbf{B}_{\text{opt}}(\mathbf{A}_L, \mathbf{G})) = &\left[(\mathbf{G}^T \otimes \mathbf{I}_3)\mathbf{S}_r(\mathbf{G} \otimes \mathbf{I}_3) + \mathbf{S}_\eta\right]^{-1} \\ &\times (\mathbf{G}^T \otimes \mathbf{I}_3)\mathbf{S}_r \text{vec}\left(\mathbf{A}_L^T\right)\end{aligned} \tag{8}$$

where vec() is an operator that transforms a matrix into a vector by stacking the columns of the matrix one underneath the other in sequence, $\mathbf{I}_3$ denotes the 3×3 identity matrix, $\otimes$ denotes the Kronecker product operator

$$\mathbf{S}_r = E\left\{(\mathbf{r}\mathbf{r}^T) \otimes \left(J_{\mathcal{F}}^T(\mathbf{t}(\mathbf{r}))J_{\mathcal{F}}(\mathbf{t}(\mathbf{r}))\right)\right\} \tag{9}$$

$$\mathbf{S}_\eta = \mathbf{K}_\eta \otimes E\left\{J_{\mathcal{F}}^T(\mathbf{t}(\mathbf{r}))J_{\mathcal{F}}(\mathbf{t}(\mathbf{r}))\right\} \tag{10}$$

and $\mathbf{K}_\eta = E\{\boldsymbol{\eta}\boldsymbol{\eta}^T\}$ is the noise covariance matrix.

The minimum mean-squared linearized color error obtained using the optimal transformation from (8) is given by

$$\xi(\mathbf{A}_L, \mathbf{G}) = \alpha(\mathbf{A}_L) - \tau(\mathbf{A}_L, \mathbf{G}) \tag{11}$$

where

$$\alpha(\mathbf{A}_L) = \text{vec}\left(\mathbf{A}_L^T\right)^T \mathbf{S}_r \text{vec}\left(\mathbf{A}_L^T\right) \tag{12}$$

$$\begin{aligned}\tau(\mathbf{A}_L, \mathbf{G}) = &\text{vec}\left(\mathbf{A}_L^T\right)^T \mathbf{S}_r(\mathbf{G} \otimes \mathbf{I}_3) \\ &\times \left[(\mathbf{G}^T \otimes \mathbf{I}_3)\mathbf{S}_r(\mathbf{G} \otimes \mathbf{I}_3) + \mathbf{S}_\eta\right]^{-1} \\ &\times \left(\mathbf{G}^T \otimes \mathbf{I}_3\right)\mathbf{S}_r \text{vec}\left(\mathbf{A}_L^T\right).\end{aligned} \tag{13}$$

A brief sketch for the derivation of (8)–(13) is included in Appendix A.[1] If the transformation $\mathcal{F}()$ is a linear transformation, significant computational savings can be made in the computation of the above expressions. Since these will be of interest in subsequent discussions, the computational simplifications for the case when $\mathcal{F}()$ is a linear transformation are summarized in Appendix B.

IV. Figures of Merit for Scanners

The error metric for scanners derived above is useful for comparing the color accuracy of different filter sets in a chosen color space, i.e., for a given $\mathcal{F}()$. Since different color spaces may have very different scales, a normalized figure of merit is more useful for the comparison of error metrics in different spaces. It can be readily seen that, in (11)

$$0 \le \tau(\mathbf{A}_L, \mathbf{G}) \le \alpha(\mathbf{A}_L).$$

The term $\alpha(\mathbf{A}_L)$ may be interpreted as the average "color" energy in a spectrum from the spectral ensemble and and $\tau(\mathbf{A}_L, \mathbf{G})$ then represents the part of this energy that is recoverable from measurements made with the scanner specified by $\mathbf{G}$ (at the given noise level). Furthermore, the "units" of this "color" energy are approximately perceptually uniform if $\mathcal{F}()$ represents the transformation from CIE XYZ space to a uniform color space. Hence, the ratio

$$q_{\mathcal{F}}(\mathbf{A}_L, \mathbf{G}) = \frac{\tau(\mathbf{A}_L, \mathbf{G})}{\alpha(\mathbf{A}_L)} \tag{14}$$

defines a normalized *figure of merit* (FOM) for the color scanner, where the subscript $\mathcal{F}$ has been added to explicitly indicate the dependence on the transformation $\mathcal{F}()$ (which was implicit in the earlier expressions). The normalization ensures that the figure of merit is bounded between zero and one with $q_{\mathcal{F}}(\mathbf{A}_L, \mathbf{G}) = 1$ representing a "perfect" color scanner whose error metric is zero.

While the discussion so far assumed the use of the scanner for colorimetry under a single viewing illuminant, the expressions are readily extended to multi-illuminant color correction problems by using appropriate weighted averages of the error metrics or figures of merit. Similar averages can be used for devices aimed at measuring both reflective and emissive objects [19], [7], [8].

A number of different color spaces and varying amounts of statistical information may be used in (14). This leads to a number of different figures of merit that have been used for the evaluation of color scanners. The following subsections discuss how these FOM's conform to the general framework developed above. Though the color quality factor does not fit the above framework, it is included in the discussion here for completeness.

A. XYZ Mean-Squared-Error-Based FOM

While it is well known that the CIE XYZ color space is perceptually nonuniform [2], the simplicity of a FOM based on MSE in CIE XYZ space is attractive. For this case, the color space transformation $\mathcal{F}()$ is, in fact, the identity mapping and, using the expressions from Appendix B, it can be readily seen that the FOM is given by

$$q_{\mathbf{I}}(\mathbf{A}_L, \mathbf{G}) = \frac{\text{tr}\left(\mathbf{A}_L^T\mathbf{K}_r\mathbf{G}(\mathbf{G}^T\mathbf{K}_r\mathbf{G} + \mathbf{K}_\eta)^{-1}\mathbf{G}^T\mathbf{K}_r\mathbf{A}_L\right)}{\text{tr}\left(\mathbf{A}_L^T\mathbf{K}_r\mathbf{A}_L\right)} \tag{15}$$

where $\text{tr}(\cdot)$ denotes the trace operator and $\mathbf{K}_r = E\{\mathbf{r}\mathbf{r}^T\}$ is the correlation matrix for the ensemble of reflectance spectra of scanned objects.

B. FOM's Based on Orthogonal Color Spaces

From a signal processing viewpoint, the use of an orthogonal color space, instead of the highly correlated CIE XYZ space, would be desirable. This can be achieved by requiring that the color space transformation $\mathcal{F}()$ is a linear transformation specified by a matrix, $\mathbf{F}_o$, such that the columns of $\mathbf{A}_L\mathbf{F}_o^T$ are orthonormal. $\mathbf{F}_o\mathbf{A}_L^T\mathbf{r}$ is then the vector of the tristimulus values of the reflectance $\mathbf{r}$ in the corresponding orthogonal color space. Once again using expressions from Appendix B,

[1] Since the submission of this paper, the authors have become aware of [18], where an equation equivalent to (8) has been derived from a different motivation.

it can be seen that in this case the FOM is given by

$$q_o(\mathbf{A}_L, \mathbf{G}) = \frac{\mathrm{tr}(\mathbf{P}_{\mathbf{A}_\mathbf{L}}\mathbf{K}_r\mathbf{G}(\mathbf{G}^T\mathbf{K}_r\mathbf{G}+\mathbf{K}_\eta)^{-1}\mathbf{G}^T\mathbf{K}_r)}{\mathrm{tr}(\mathbf{P}_{\mathbf{A}_\mathbf{L}}\mathbf{A}_L^T\mathbf{K}_r)} \tag{16}$$

where $\mathbf{P}_{\mathbf{A}_\mathbf{L}} = \mathbf{A}_L\mathbf{F}_o^T\mathbf{F}_o\mathbf{A}_L^T$ is the orthogonal projector onto the column-space of $\mathbf{A}_L$, known as the *human visual illuminant subspace* (HVISS) [4].

Observe that the above FOM is independent of the choice of the orthonormalizing transformation $\mathbf{F}_o$ and of the actual columns of $\mathbf{A}_L$ (depending only on their span instead). Since the choice of particular CIE XYZ color matching functions to represent the human visual space was made for mathematical convenience and not for any reasons of perceptual uniformity [1], [2], this independence is a desirable feature. It may also be noted that Vrhel and Trussell [9], [10] formulated the problem of designing color scanning filters in terms of the maximization of the numerator in (16) and thus implicitly used the above FOM.

If measurement noise is ignored, i.e., it is assumed that $\mathbf{K}_\eta = \mathbf{0}$, the figure of merit in (16) reduces to the data-dependent measure of goodness for color scanning filters proposed by Vora [20, p. 90]. If in addition, the "maximum ignorance assumption" is used for the spectral correlation matrix of the reflectance spectra of the scanned ensemble, i.e., it is assumed that $\mathbf{K}_r$ is a scalar multiple of the identity, the FOM reduces to the data independent Vora measure for color scanning filters [4]

$$q_v(\mathbf{A}_L, \mathbf{G}) = \frac{\mathrm{tr}(\mathbf{P}_{\mathbf{A}_\mathbf{L}}\mathbf{P}_\mathbf{G})}{3} \tag{17}$$

where $\mathbf{P}_\mathbf{G} = \mathbf{G}(\mathbf{G}^T\mathbf{G})^{-1}\mathbf{G}^T$ is the orthogonal projector onto the column-space of $\mathbf{G}$, defined as the *scanner visual subspace* (SVS).

C. Neugebauer's Quality Factor

If the scanner has orthogonal channels, i.e., $\mathbf{G} = [\mathbf{g}_1\mathbf{g}_2 \ldots \mathbf{g}_K]$, with $\mathbf{g}_i^T\mathbf{g}_j = 0$, $i \neq j$, the Vora measure can be rewritten as

$$q_v^1(\mathbf{A}_L, \mathbf{G}) = \frac{1}{3}\sum_{i=1}^{K}\frac{\|\mathbf{P}_{\mathbf{A}_\mathbf{L}}\mathbf{g}_i\|^2}{\|\mathbf{g}_i\|^2}. \tag{18}$$

The above expression can be interpreted as the normalized sum of the goodness measures of the individual scanning filters. This goodness measure is, in fact, the quality factor for filters proposed by Neugebauer [3]

$$q_n(\mathbf{A}_L, \mathbf{g}) = \frac{\|\mathbf{P}_{\mathbf{A}_\mathbf{L}}\mathbf{g}\|^2}{\|\mathbf{g}\|^2}. \tag{19}$$

For filter sets with orthogonal or nearly orthogonal filters, the average of the Neugebauer quality factors is a reasonable measure of goodness for the set. However, for nonorthogonal filters the use of average quality factors can lead to gross mispredictions [4]. Since the Vora measure covers the useful case of orthogonal filters, the Neugebauer quality factor will not be considered in the subsequent discussion.

D. Color Quality Factor

The Vora measure attempts to quantify the "fraction" of the HVISS contained in the SVS. The Neugebauer quality factor, on the other hand, attempts to evaluate single filters by determining the fraction of the filters energy that lies in the HVISS. By reversing the roles of the HVISS and the SVS, one can determine what fraction of the energy of each illuminant-color-matching-function product lies within the SVS. Thus if the illuminant-color-matching-function product matrix is written in terms of its columns as $\mathbf{A}_L = [\mathbf{a}_1\mathbf{a}_2\mathbf{a}_3]$, the three factors

$$\phi(\mathbf{a}_i, \mathbf{G}) = \frac{\|\mathbf{P}_\mathbf{G}\mathbf{a}_i\|^2}{\|\mathbf{a}_i\|^2} \quad i = 1, 2, 3 \tag{20}$$

quantify the accuracy of the scanner in matching the illuminant-color-matching-function products $\mathbf{a}_1, \mathbf{a}_2, \mathbf{a}_3$, respectively. Note that these factors depend on the particular basis $\{\mathbf{a}_i\}_{i=1}^3$ chosen for the HVISS.

The minimum of the three factors $\{\phi(\mathbf{a}_i, \mathbf{G})\}_{i=1}^3$ may be chosen as a measure of the overall accuracy of the scanner in approximating the HVISS. This measure is the CQF [5]

$$q_c(\mathbf{A}_L, \mathbf{G}) = \min_{i=1,2,3}\phi(\mathbf{a}_i, \mathbf{G}). \tag{21}$$

Instead of the minimum, an average value may also be used to obtain an alternate color quality factor.

E. FOM's Based on Perceptual Color Spaces

Since scanned images are ultimately viewed by a human observer, an error metric quantifying perceived differences in color would be ideal for evaluating the scanner. Euclidean distances in the CIE XYZ space and in the orthogonal color spaces of Section IV-B agree poorly with perceived color differences and are, therefore, nonuniform color spaces from a perceptual standpoint. Several approximately uniform color spaces have been defined by the CIE [1] in which equal Euclidean distances correspond roughly to the same perceived difference in color. These spaces are described by nonlinear transformations, $\mathcal{F} : R^3 \rightarrow R^3$, that transform color tristimulus values in CIE XYZ space to the uniform color space. Typically, the transformation $\mathcal{F}()$ is differentiable with continuous first partial derivatives and therefore can be incorporated in the framework of Section III. For the purposes of this discussion, the most extensively used uniform color space, CIELAB, will be considered. The transformation $\mathcal{F}()$ and its Jacobian matrix for the CIE L*a*b* space is summarized in Appendix C. Using these expressions, a FOM for the scanner can be computed as in (14). This FOM will be denoted as $q_{pn}(\mathbf{A}_L, \mathbf{G})$, and referred to as the *perceptual FOM*. If the noise is ignored, i.e., it is assumed $\mathbf{K}_\eta = \mathbf{0}$, this figure of merit reduces to one that was implicit in Wolski *et al.*'s formulation of the filter design problem. The corresponding FOM will be referred to as the perceptual measure, $q_p(\mathbf{A}_L, \mathbf{G})$, in subsequent discussions.

It can be inferred from (13) that the computation of the perceptual FOM's is considerably more involved than the computation of the other measures for which $\mathcal{F}()$ was a linear transformation. To obtain less computationally expensive

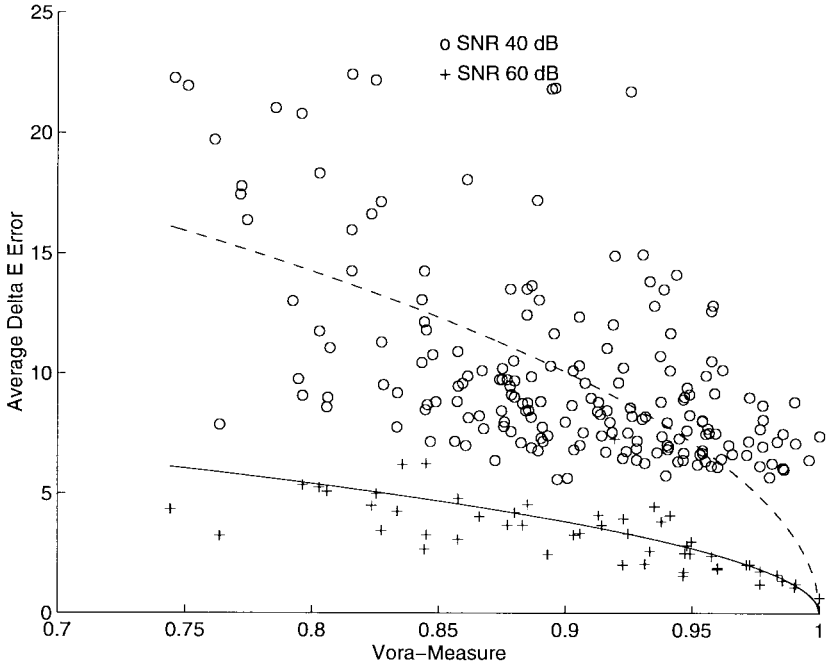

Fig. 1. Vora measure versus average $\triangle E^*_{ab}$.

FOM's, global as opposed to local linearizations of the uniform color space may be considered. One such linearization, based on the first-order Taylor series for the CIELAB space about the white point, will be considered here. Such a linearization is equivalent to replacing $\mathcal{F}()$ by a linear transformation $\mathbf{F}_{Lab}$ obtained by evaluating the Jacobian matrix of $\mathcal{F}()$ at the white point. The expression for $\mathbf{F}_{Lab}$ is given in (43) in Appendix C. The FOM obtained using this expression is given by (see Appendix B)

$$q_{apn}(\mathbf{A}_L, \mathbf{G}) = \frac{\mathrm{tr}\left(\mathbf{F}_{Lab}^T \mathbf{F}_{Lab} \mathbf{A}_L^T \mathbf{K}_r \mathbf{G} (\mathbf{G}^T \mathbf{K}_r \mathbf{G} + \mathbf{K}_\eta)^{-1} \mathbf{G}^T \mathbf{K}_r \mathbf{A}_L\right)}{\mathrm{tr}\left(\mathbf{F}_{Lab}^T \mathbf{F}_{Lab} \mathbf{A}_L^T \mathbf{K}_r \mathbf{A}_L\right)} \tag{22}$$

and will be referred to as the approximate perceptual FOM. A version of this FOM in which the noise was neglected ($\mathbf{K}_\eta = \mathbf{0}$), was implicitly used by Wolski *et al.* [7], and will be called the approximately perceptual measure $q_{ap}(\mathbf{A}_L, \mathbf{G})$.

V. Discussion

Color errors in scanners arise from two distinct sources: i) the "difference" between the HVISS and the SVS, and ii) the noise in scanner measurements. The different FOM's described in the last section were attempts at quantifying these errors. The FOM's that ignored device noise and concentrated only on the the first source of errors are referred to as *(scanner filter goodness) measures*, using terminology borrowed from [4].

In the absence of noise, the scanner measurements yield the projection of the scanned object spectra onto the SVS. If the HVISS is contained in the SVS, this projection is sufficient for exact color reproduction. The scanner measures of the last section, attempt to quantify the fractional "amount" of the HVISS that is contained in the SVS. The Vora measure and CQF are based on purely geometric ideas of the distance between subspaces [4], and ignore both the statistics of the scanned spectra and perceptual nonuniformities in the HVISS. The data-dependent Vora measure incorporates the statistics of the scanned spectra while continuing to ignore perceptual effects. The approximate perceptual measure and the perceptual measure of Section IV-E incorporate the statistics of the scanned spectra and varying degrees of perceptual information.

Since the scanner measures ignore device noise, they offer little insight on the noise performance of different filter sets for color scanning. It can be shown [15] that the measures of the last section depend only on the SVS, i.e., the space spanned by the columns of $\mathbf{G}$, and not on the individual entries in $\mathbf{G}$. Thus, they do not distinguish between different scanners having the same SVS. Since measurement noise may have significantly different impact on scanners having the same SVS but different filters, this is a significant shortcoming of the measures, which is overcome in the more comprehensive FOM's that include noise in the analysis. In a manner analogous to the scanner measures, these used varying amounts of statistical information about the scanner target ensemble and the knowledge of perceptual nonuniformities in the HVISS.

The usefulness of the different measures and FOM's for practical problems is determined by their computational requirements and by their relation to perceived color errors. These questions are investigated in the next two sections.

VI. Computational Complexity

For a one-time evaluation of an existing scanner, the cost of computing the different FOM's is not important. However, if the problem of designing an optimal color scanner is formulated as the maximization of the FOM, the cost of computing the FOM is a significant issue. The computational

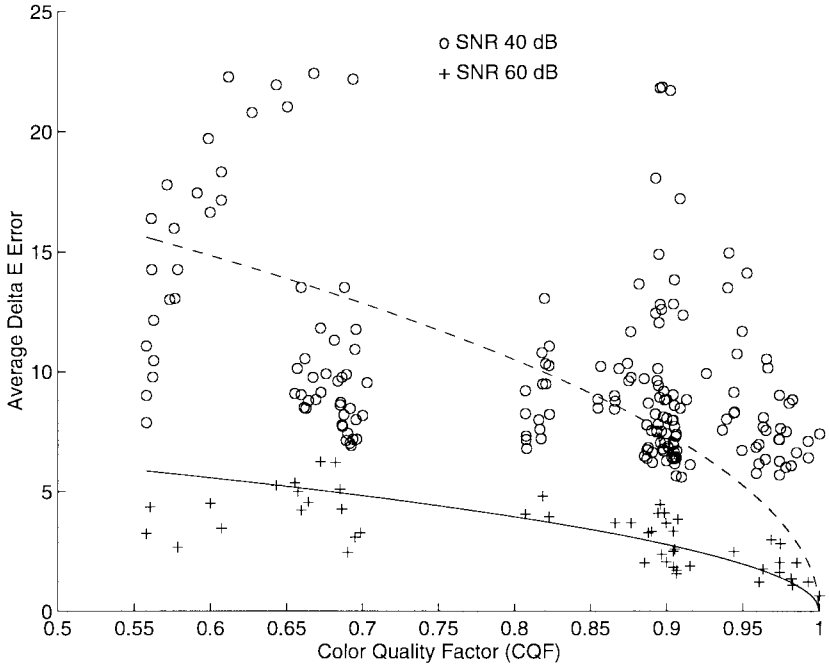

Fig. 2. CQF versus average $\triangle E^*_{ab}$.

complexity of the different FOM's is therefore analyzed in this section.

Note that the normalization factor $\alpha(\mathbf{A}_L)$ in (14) does not depend on $\mathbf{G}$ and, therefore, needs to be computed only once. The same is true of the statistical information regarding the scanner target ensemble and the noise, contained in the matrices $\mathbf{S}_r$, $\mathbf{S}_\eta$, $\mathbf{K}_r$, and $\mathbf{K}_\eta$. These costs will therefore not be considered as part of the computational requirements of the different FOM's.

By using the special structure of the matrices, significant savings can be made in the computation of the different FOM's and measures. Usually, the noise in different channels is uncorrelated and $\mathbf{K}_\eta$ is a diagonal matrix. Therefore, in the evaluation of computational requirements, it will be assumed that $\mathbf{K}_\eta$ is diagonal. The matrices $\mathbf{S}_r$, $\mathbf{S}_\eta$, $\mathbf{K}_r$, and $\mathbf{K}_\eta$ are symmetric positive definite matrices. These properties are therefore inherited by the matrices whose inverses occur in (13), (15), (16), and (22). Using this observation, it can be seen that each of these FOM's can be written in the form $\mathrm{tr}(\mathbf{U}^T\mathbf{W}^{-1}\mathbf{U})/\alpha$ where α is a normalizing constant (independent of $\mathbf{G}$), $\mathbf{W}$ is a context-dependent positive definite matrix and $\mathbf{U}$ is another context dependent matrix (or a vector). Let $\mathbf{W} = \mathbf{V}\mathbf{V}^T$ denote the Cholesky factorization [16] of $\mathbf{W}$, where $\mathbf{V}$ is a lower triangular matrix. The aforementioned measures are computed most efficiently using the fact that

$$\mathrm{tr}(\mathbf{U}^T\mathbf{W}^{-1}\mathbf{U}) = \|\mathbf{V}^{-1}\mathbf{U}\|_F^2 \tag{23}$$

where $\|\cdot\|_F$ denotes the Frobenius norm [16]. Using (23), it can be seen [16] that the computation of each of the XYZ MSE-based FOM, the FOM's based on orthogonal color spaces, and the approximate perceptual FOM's of (15), (16), and (22) requires $2NK(N+K+6)+K^3/3+(7K^2)/2+(37K)/6$ floating point operations (FLOP's); and the computation of the perceptual FOM based on (13) requires $18NK(3(N+K)+1)+9K^3+(45K^2)/2+(13K)/2$ FLOP's. The scanner goodness measures obtained by ignoring noise in these FOM's require roughly the same number of computations as the FOM's themselves.

The Vora measure in (17) can be computed in a stable and efficient manner by using the QR factorization [16] to obtain orthonormal bases, $\mathbf{N}$ and $\mathbf{O}$, for the column spaces of $\mathbf{A}_L$ and $\mathbf{G}$, respectively. The Vora measure can then be computed as $\|\mathbf{N}^T\mathbf{O}\|_F^2/3$. This requires $2NK(K+3) - (2K^3)/3 + 7K$ FLOP's. Using the same idea, the color quality factor in (21) can be written as $\min\|\mathbf{O}^T\mathbf{a}_i\|^2/\|\mathbf{a}_i\|^2$ and requires $2NK(K+1) - (2K^3)/3 + 3K$ FLOP's.

Typically, a 10 nm sampling interval is used for color spectra over the visible range 390 nm to 730 nm, yielding $N = 35$ samples for the various spectral terms. Since color scanners and cameras use only a few channels, K is relatively small in relation to N (typically K is between 3 and 7 [10]). Hence, the N^2 term in the above expressions is computationally the dominant term. Using this observation, it can readily be seen that the Vora measure and CQF are computationally the most simple, requiring far fewer FLOP's than the other FOM's. The FOM's based on MSE in CIE XYZ space, the orthogonal color spaces, or the globally linearized CIELAB space are next in order of increasing computational complexity, and all require the same number of FLOP's. The perceptual FOM is computationally the most expensive and requires roughly $3^3 = 27$ times the computation of the FOM's based on global linear transformations of the CIE XYZ space. For the typical case of $N = 35$, and for values of K between 3 and 7, the computational requirements for the different FOM's (computed using the general expressions involving N and K)

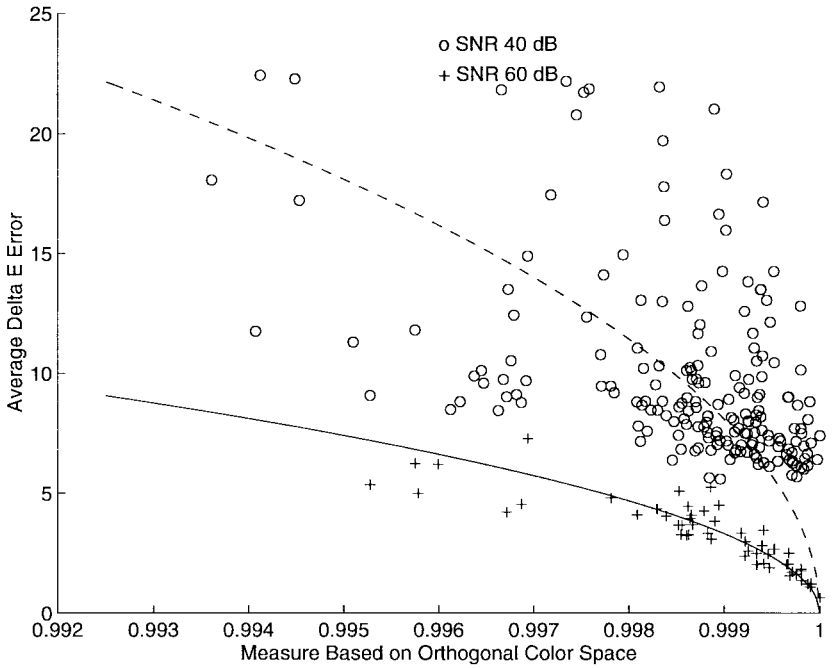

Fig. 3. Data-dependent Vora measure versus average $\triangle E^*_{ab}$.

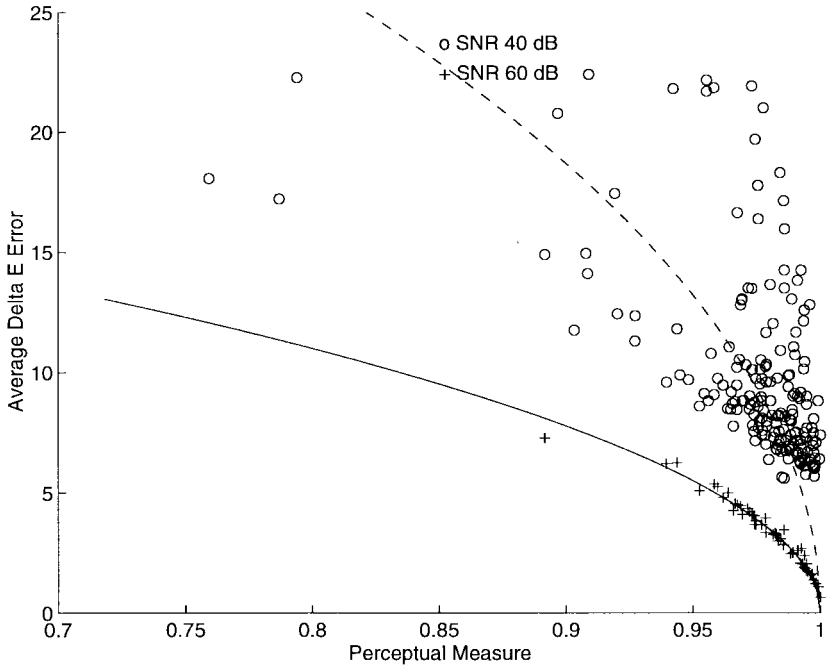

Fig. 4. Perceptual measure versus average $\triangle E^*_{ab}$.

are listed in Table I. The table facilitates a comparison of the relative computational requirements of the different FOM's.

VII. Experimental Results

Since color is finally judged by a human observer, the average perceptual color error over the ensemble of scanned spectra is an ideal metric for evaluating color scanners. A FOM that is monotonically related to the average perceptual error is equally useful. Hence, the nature of the relation between the average perceptual error and a FOM can be used to evaluate the trustworthiness of the FOM. Since perceived errors are psychophysical and cannot be evaluated without extensive experimentation, in this section, a quantitative specification of color errors is considered using a perceptually uniform color space. In particular, the Euclidean distance in CIELAB space (L*a*b*), referred to as the $\triangle E^*_{ab}$ error, will be used as an approximation to the magnitude of perceived color error.

The predictive abilities of different FOM's can be evaluated by examining the relationship between the FOM and the average $\triangle E^*_{ab}$ error over the scanner target ensemble for a

TABLE I
COMPUTATIONAL REQUIREMENTS OF THE FOM'S FOR $N = 35$

FOM or Measure	FLOPS ($\times 10^3$)				
	$K = 3$	$K = 4$	$K = 5$	$K = 6$	$K = 7$
CQF	0.831	1.369	2.032	2.814	3.712
Vora	1.263	1.945	2.752	3.678	4.720
Linear $\mathcal{F}()$	9.299	12.702	16.260	19.975	23.849
Nonlinear $\mathcal{F}()$	217.815	298.322	382.870	471.513	564.305

number of filter sets. Simulations were performed to determine this relationship for the different FOM's. Throughout the simulations, a 10 nm sampling interval was used over the wavelength range 390–730 nm so that there were $N = 35$ samples for each spectrum. It was assumed that the scanning and the viewing illuminants are the CIE daylight illuminant D65 [1], [2], so that $\mathbf{L}$ and $\mathbf{L_s}$ are identical. With this assumption, in the absence of noise the CIE XYZ color matching functions define a "perfect" filter set with unity Vora measure. Parameterized filter sets were used to obtain a large number of additional filter sets with varying FOM's. The filter sets were designed to have three filters in each set. The spectral transmittance of each filter was specified by a Gaussian function of the form $\exp(-(\lambda-\mu)^2/(2\gamma^2))$, where λ denotes wavelength; and the mean, μ, and the variance, γ^2, are the parameters specifying the filter. A "base set" of Gaussian filters was created by determining the means and variances of the three filters so as to maximize the Vora measure. Both the means and standard deviations (square-roots of the variances) defining the filters were then varied within 40 nm bands about their "optimal values" to obtain a number of filter sets. The filter sets in which the filter transmittances were nearly linearly dependent were dropped. This procedure yielded a total of 251 filter sets spanning a significant range of Vora measures. It may be noted that the results presented here are essentially unchanged if other combinations of smooth viewing and scanning illuminants, such as CIE incandescent illuminant A, daylight illuminant D50, or the equal energy illuminant E [1], [2] are used in the simulations.

The simulations used an ensemble of scanner target reflectances containing 424 reflectances. Of these, 240 were from the Kodak Q60 Photographic Scanner Target [21], 64 from the Munsell chart, and 120 from a Dupont paint catalog [22]. Simulated noisy measurements were made with each filter set for the entire ensemble using (3). The measurement noise $\boldsymbol{\eta}$ was assumed to be signal-independent, zero-mean, white, Gaussian noise with (per-channel) variance σ_η^2 determined by the signal-to-noise ratio (SNR) defined as

$$\text{SNR (dB)} = 10\log_{10}\left(\frac{\text{tr}(\mathbf{G}^T\mathbf{K}_r\mathbf{G})}{\sigma_\eta^2}\right). \tag{24}$$

The noise correlation matrix was thus $\mathbf{K}_\eta = \sigma_\eta^2\mathbf{I}$. Sample averages over the ensemble of reflectances were used to estimate the matrices $\mathbf{S}_r$, $\mathbf{K}_r$, and $\mathbf{S}_\eta$. These were then used to determine the "optimal transformation" of (7) for each filter set. Using this transformation, CIE XYZ tristimulus values were estimated from each simulated noisy scanner measurement. Actual CIE XYZ values corresponding to the same reflectance were also computed using (1). The actual and estimated tristimulus values were transformed to CIELAB space, and the Euclidean distance was computed between them to obtain the $\triangle E_{ab}^*$ error corresponding to a single reflectance. For each filter set, the mean of these errors over the entire ensemble of scanner target reflectance spectra was computed to obtain an average $\triangle E_{ab}^*$ error corresponding to the filter set. For each filter set, the different FOM's of Section IV were also computed. The relationship of each FOM to the average $\triangle E_{ab}^*$ error was examined by using a scatter plot of the two quantities for the 251 filter sets. SNR values of 40, 50, and 60 dB were considered in the simulations.

The relation between the different scanner measures (that ignore noise) and the average $\triangle E_{ab}^*$ error is illustrated in the scatter plots of Figs. 1–4. Only a representative random selection of the 251 points corresponding to the different filter sets has been included in these and subsequent plots to keep them uncluttered. Also included in all the plots are best fit curves of the form, $avg.\triangle E_{ab}^* = \beta\sqrt{1-FOM}$. The rationale behind such a curve comes from (14), where it can be seen that the FOM's have the corresponding square-root relation to a root-mean-squared color error. From the figures, it can be seen that the CQF does not have the desired approximately monotonic relation to the average $\triangle E_{ab}^*$ error even at a relatively high SNR of 60 dB. At the same SNR, the Vora measure does somewhat better, the data-dependent Vora measure makes significant gains over the Vora-measure by incorporating knowledge of the correlation of scanned spectra, and the perceptual measure does extremely well, with all the points in the scatter plot lying very close to a smooth monotonic curve. At an SNR of 40 dB, significant changes occur in each of the scatter plots. For all the measures, there is apparently no clear functional relationship between the measures and the average $\triangle E_{ab}^*$ error. Also note that, even at the moderately high SNR of 40 dB, the measure 1 filters (the CIE XYZ color matching functions) are no longer optimal from a perceptual standpoint. Several interesting facts can also be observed from the abscissa of the different plots. Because of the use of the minimum in (21), the CQF is often lower than other measures, providing pessimistic estimates even in the absence of noise. The data-dependent measures are rather high for all the filter sets. An explanation for this can be found in the fact that object reflectance spectra can be well approximated by a low-dimensional space [22]. In the limiting case, when the scanned reflectances lie in an M-dimensional space, it can be seen that the data-dependent measures are unity for any scanner with M or more linearly independent channels [23].

Figs. 5–8 demonstrate the relation between the different FOM's that account for device noise and the average $\triangle E_{ab}^*$ error. From Fig. 5, it is clear that the CIE XYZ MSE-based FOM is a poor indicator of perceptual color error. The poor predicted performance for the cluster of points below the solid curve in the center of the figure is probably due to the computation of errors in a nonorthogonal space. The FOM

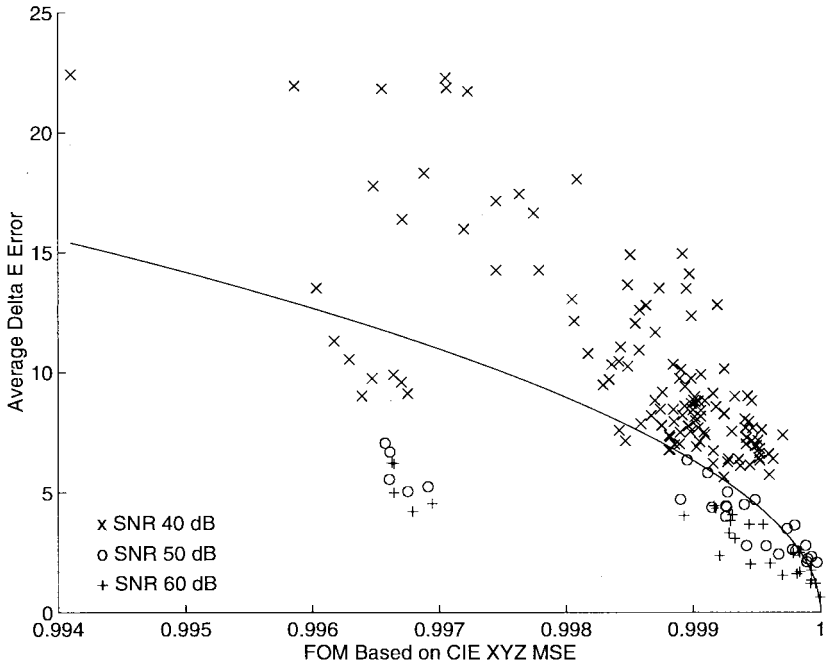

Fig. 5. CIE XYZ-based FOM versus average $\triangle E^*_{ab}$.

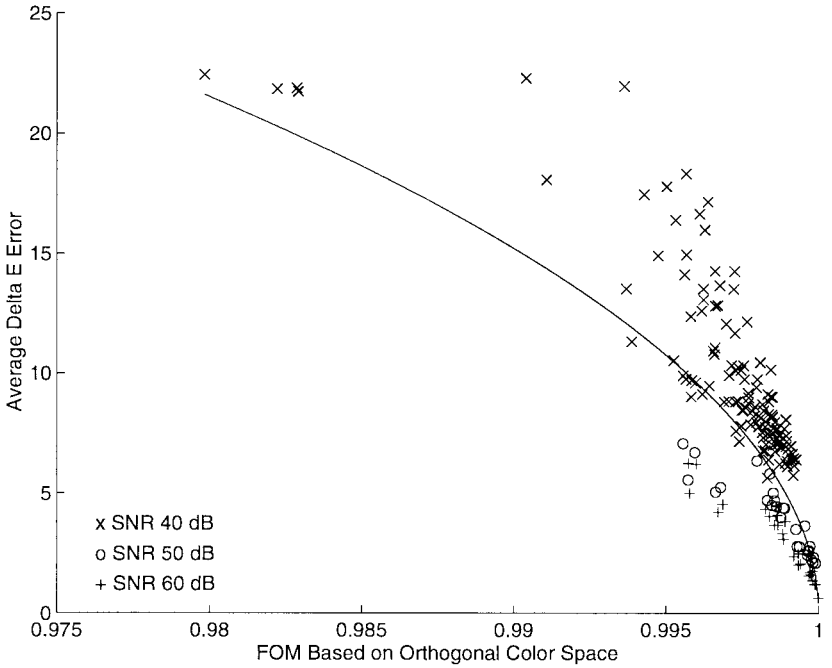

Fig. 6. Orthogonal color space based FOM versus average $\triangle E^*_{ab}$.

based on an orthogonal color space is considered in Fig. 6 and the approximately perceptual FOM based on a global linearization of CIELAB space in Fig. 7. From the plots, it is clear that these FOM's are better indicators of perceived color error than the CIE XYZ MSE-based FOM. However, the points constituting the scatter diagrams are far from a smooth monotonic curve in either case. Fig. 8 is the scatter plot corresponding to the perceptual FOM. The points in this case are almost ideally distributed, lying along a rather well-defined smooth monotonic curve. Note that unlike the measures that did not vary with SNR, the perceptual FOM has lower values at lower SNR's and the corresponding points on the scatter diagram are shifted to the left, forming a continuous smooth curve. Thus, the perceptual FOM also captures the tradeoff between the errors arising due to the difference in the HVISS and the SVS and those arising due to the device noise, providing an ideal FOM for analysis and design of color scanners and cameras.

Since several applications require that the worst case color errors be minimized, it is also desirable to have a monotonic

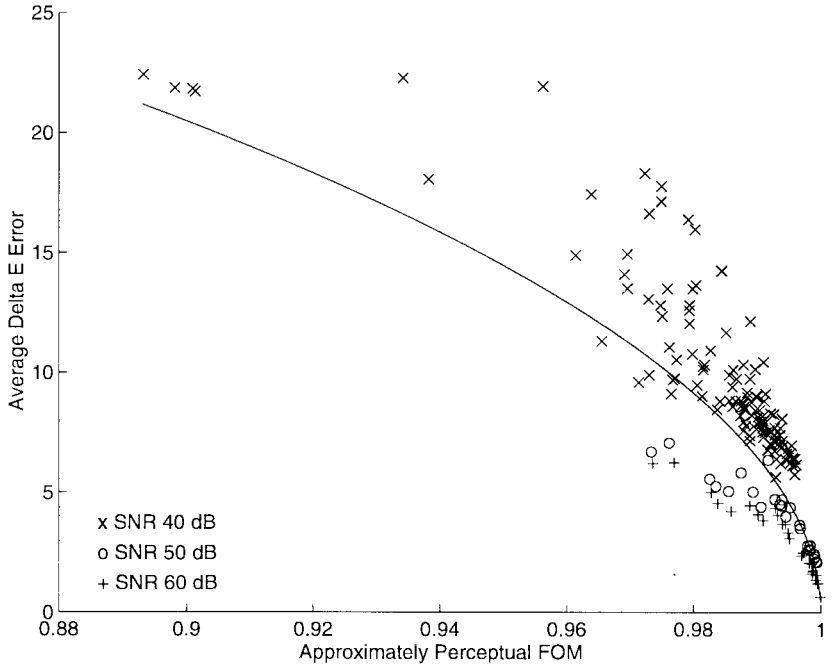

Fig. 7. Approximate perceptual FOM versus average $\triangle E^*_{ab}$.

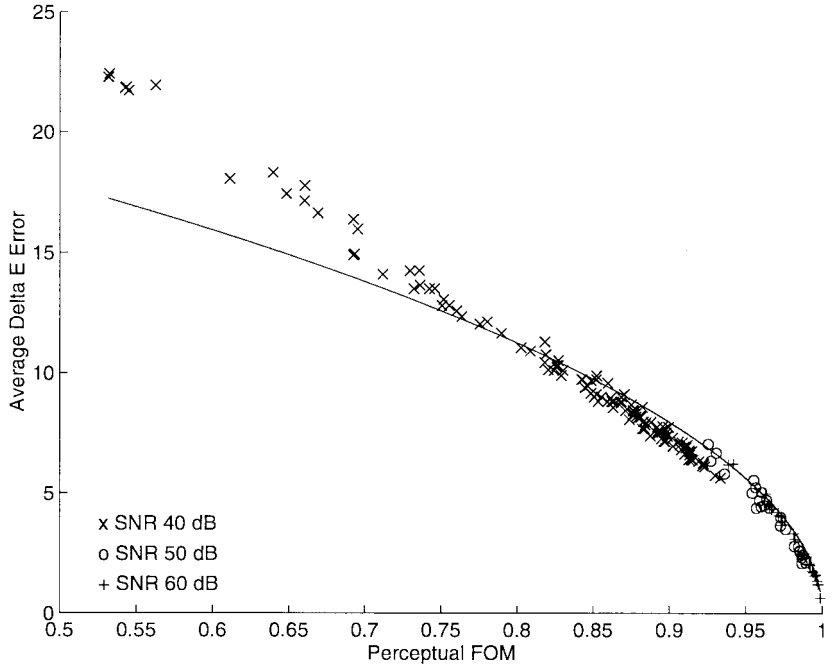

Fig. 8. Perceptual FOM versus average $\triangle E^*_{ab}$.

decrease in the maximum $\triangle E^*_{ab}$ error with increase in an FOM. A scatter plot of the maximum $\triangle E^*_{ab}$ error (over the ensemble of 424 reflectances) versus the perceptual FOM is shown in Fig. 9. The points constituting the scatter diagram have considerably larger spread than the corresponding diagram for the average $\triangle E^*_{ab}$ error. Since the FOM was based on mean-squared values, this larger spread is to be expected. However, note that the monotonic trend is still apparent, particularly for filter sets with a high (perceptual) FOM. This is encouraging, since it indicates that for scanners with reasonably high perceptual FOM, the FOM also reflects the worst case performance with fair accuracy.

VIII. Conclusion

In this paper, a unified framework was developed for the description of several figures of merit (FOM's) for color scanning systems. A new perceptual FOM was obtained using linear approximations to CIELAB space, which accounted for color errors from the noncolorimetric design of scanning filters as well as the errors resulting from measurement noise. The

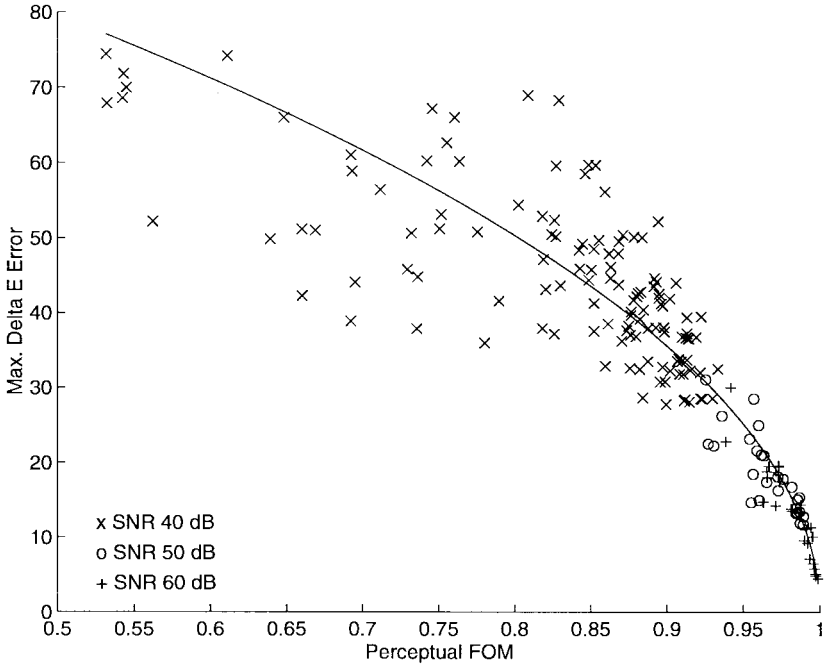

Fig. 9. Perceptual FOM versus maximum $\triangle E^*_{ab}$.

computational requirements of different FOM's were analyzed. The relation between the different FOM's and perceptual error was studied through simulations. The new perceptual figure of merit was shown to be in excellent agreement with perceived color error (quantified in terms of the average $\triangle E^*_{ab}$ error) for filter sets with considerable variation in colorimetric accuracy and across a wide range of SNR values.

Appendix A
Derivation of the Generalized Error Metric

In this appendix, a brief derivation of (8)–(13) leading to the general scanner error metric is provided. For this purpose, it is useful to introduce the $\mathrm{vec}(\cdot)$ operator that transforms a matrix into a vector by stacking the columns of the matrix one underneath the other in sequence. It is also useful to state some properties of the $\mathrm{vec}(\cdot)$ operator and the Kronecker product. For arbitrary matrices, $\mathbf{T}$, $\mathbf{U}$, $\mathbf{V}$, and $\mathbf{W}$, the following results [17, pp. 27–30] hold:

$$\mathrm{vec}(\mathbf{UVW}) = (\mathbf{W}^T \otimes \mathbf{U})\mathrm{vec}(\mathbf{V}) \tag{25}$$

$$(\mathbf{T}+\mathbf{U}) \otimes (\mathbf{V}+\mathbf{W}) = \mathbf{T}\otimes\mathbf{V} + \mathbf{T}\otimes\mathbf{W} + \mathbf{U}\otimes\mathbf{V} + \mathbf{U}\otimes\mathbf{W} \tag{26}$$

$$(\mathbf{T}\otimes\mathbf{U})(\mathbf{V}\otimes\mathbf{W}) = \mathbf{TV}\otimes\mathbf{UW} \tag{27}$$

$$(\mathbf{T}\otimes\mathbf{U})^T = (\mathbf{T}^T \otimes \mathbf{U}^T) \tag{28}$$

where $\otimes$ denotes the Kronecker product and it is assumed that the matrices satisfy appropriate size restrictions for all the operations to be defined.

Substituting (3) in (6)

$$\epsilon_l(\mathbf{A_L}, \mathbf{G}, \mathbf{B}) = E\{\left|\left|J_{\mathcal{F}}(\mathbf{t}(\mathbf{r}))\left[\mathbf{A}_\mathbf{L}^T\mathbf{r} - \mathbf{B}(\mathbf{G}^T\mathbf{r}+\boldsymbol{\eta})\right]\right|\right|^2\}. \tag{29}$$

Using (25)

$$J_{\mathcal{F}}(\mathbf{t}(\mathbf{r}))\mathbf{A}_\mathbf{L}^T\mathbf{r} = (\mathbf{r}^T \otimes J_{\mathcal{F}}(\mathbf{t}(\mathbf{r})))\mathrm{vec}\left(\mathbf{A}_\mathbf{L}^T\right). \tag{30}$$

$$J_{\mathcal{F}}(\mathbf{t}(\mathbf{r}))\mathbf{B}[\mathbf{G}^T\mathbf{r}+\boldsymbol{\eta}] = [(\mathbf{G}^T\mathbf{r}+\boldsymbol{\eta})^T \otimes J_{\mathcal{F}}(\mathbf{t}(\mathbf{r}))]\mathrm{vec}(\mathbf{B}). \tag{31}$$

Denoting $\mathbf{b} = \mathrm{vec}(\mathbf{B})$, $\mathbf{x} = (\mathbf{r}^T \otimes J_{\mathcal{F}}(\mathbf{t}(\mathbf{r})))\mathrm{vec}(\mathbf{A}_\mathbf{L}^T)$, and $\mathbf{Y} = [(\mathbf{G}^T\mathbf{r}+\boldsymbol{\eta})^T \otimes J_{\mathcal{F}}(\mathbf{t}(\mathbf{r}))]$

$$\begin{aligned}\epsilon_l(\mathbf{A_L}, \mathbf{G}, \mathbf{B}) &= E\{||\mathbf{x}-\mathbf{Yb}||^2\} \\ &= E\{||\mathbf{x}||^2\} - 2E\{\mathbf{x}^T\mathbf{Y}\}\mathbf{b} + \mathbf{b}^T E\{\mathbf{Y}^T\mathbf{Y}\}\mathbf{b}.\end{aligned} \tag{32}$$

It readily follows [16] that

$$\begin{aligned}\mathrm{vec}(\mathbf{B}_{\mathrm{opt}}(\mathbf{A}_L, \mathbf{G})) &\equiv \arg\min_{\mathbf{B}} \epsilon_l(\mathbf{A}_L, \mathbf{G}, \mathbf{B}) \\ &= [E\{\mathbf{Y}^T\mathbf{Y}\}]^{-1}E\{\mathbf{Y}^T\mathbf{x}\}\end{aligned} \tag{33}$$

and

$$\begin{aligned}&\epsilon_l(\mathbf{A_L}, \mathbf{G}, \mathbf{B}_{\mathrm{opt}}) \\ &\quad = E\{||\mathbf{x}||^2\} - E\{\mathbf{x}^T\mathbf{Y}\}[E\{\mathbf{Y}^T\mathbf{Y}\}]^{-1}E\{\mathbf{Y}^T\mathbf{x}\}.\end{aligned} \tag{34}$$

If the measurement noise $\boldsymbol{\eta}$ is zero mean and independent of $\mathbf{r}$, then (8)–(13) are readily obtained [15] by simplifying $E\{||\mathbf{x}||^2\}$, $E\{\mathbf{Y}^T\mathbf{x}\}$, and $E\{\mathbf{Y}^T\mathbf{Y}\}$ using properties (26)–(28).

Appendix B
Simplifications for Linear $\mathcal{F}()$

In this appendix, simplifications for the expressions in (9)–(13) are considered for the case when the color space transformation $\mathcal{F}()$ is a linear transformation specified by a matrix $\mathbf{F}$. Then it can be readily seen that $\mathbf{S}_r = \mathbf{K}_r \otimes (\mathbf{F}^T\mathbf{F})$, and $\mathbf{S}_\eta = \mathbf{K}_\eta \otimes (\mathbf{F}^T\mathbf{F})$, where $\mathbf{K}_r = E\{\mathbf{r}\mathbf{r}^T\}$ is the correlation matrix for the ensemble of reflectance spectra of scanned objects.

Using these expressions, and the properties of the Kronecker product, it can be shown that [15]

$$\mathbf{B}_{\text{opt}}(\mathbf{A}_L, \mathbf{G}) = \mathbf{A}_L^T(\mathbf{G}^T\mathbf{K}_r\mathbf{G} + \mathbf{K}_\eta)^{-1}\mathbf{G}^T\mathbf{K}_r \tag{35}$$

$$\begin{aligned}\alpha(\mathbf{A}_L) &= \text{vec}\big(\mathbf{A}_L^T\big)^T[\mathbf{K}_r \otimes \mathbf{F}^T\mathbf{F}]\text{vec}\big(\mathbf{A}_L^T\big) \\ &= \text{tr}\big(\mathbf{F}^T\mathbf{F}\mathbf{A}_L^T\mathbf{K}_r\mathbf{A}_L\big)\end{aligned} \tag{36}$$

$$\begin{aligned}\tau(\mathbf{A}_L, \mathbf{G}) &= \text{vec}\big(\mathbf{A}_L^T\big)^T[\mathbf{K}_r\mathbf{G}(\mathbf{G}^T\mathbf{K}_r\mathbf{G} + \mathbf{K}_\eta)^{-1} \\ &\quad \times \mathbf{G}^T\mathbf{K}_r \otimes \mathbf{F}^T\mathbf{F}]\text{vec}\big(\mathbf{A}_L^T\big) \\ &= \text{tr}(\mathbf{F}^T\mathbf{F}\mathbf{A}_L^T\mathbf{K}_r\mathbf{G}(\mathbf{G}^T\mathbf{K}_r\mathbf{G} + \mathbf{K}_\eta)^{-1} \\ &\quad \times \mathbf{G}^T\mathbf{K}_r\mathbf{A}_L)\end{aligned} \tag{37}$$

where $\text{tr}(\cdot)$ denotes the trace operator.

Note that $\mathbf{B}_{\text{opt}}(\mathbf{A}_L, \mathbf{G})$ does not depend on $\mathbf{F}$ (this is not true in general for a nonlinear transformation $\mathcal{F}()$). However, the scanner error metric $\xi(\mathbf{A}_L, \mathbf{G})$ still depends on $\mathbf{F}$.

APPENDIX C
LINEARIZATIONS OF CIELAB SPACE

For the CIELAB color space the transformation $\mathcal{F}()$ is given by [1]

$$\mathcal{F}(\mathbf{t}) = \begin{bmatrix} 116f\big(\frac{t_2}{w_2}\big) - 16 \\ 500\big(f\big(\frac{t_1}{w_1}\big) - f\big(\frac{t_2}{w_2}\big)\big) \\ 200\big(f\big(\frac{t_2}{w_2}\big) - f\big(\frac{t_3}{w_3}\big)\big) \end{bmatrix} \tag{38}$$

where

$$f(x) = \begin{cases} x^{\frac{1}{3}} & x > 0.008\,856 \\ 7.787x + \frac{16}{116} & x \le 0.008\,856 \end{cases} \tag{39}$$

and $\mathbf{w} = [w_1, w_2, w_3]^T$ denotes the CIE XYZ tristimulus values of the white point. The tristimulus values of the perfect reflector (spectral reflectance unity at all wavelengths) will be considered at the white point in this paper.

The Jacobian matrix of the transformation $\mathcal{F}()$ is given by

$$\mathbf{J}_{\mathcal{F}}(\mathbf{t}) = \mathbf{J}_0\mathbf{D}(\mathbf{t}) \tag{40}$$

where

$$\mathbf{J}_0 = \begin{bmatrix} 0 & 116 & 0 \\ 500 & -500 & 0 \\ 0 & 200 & -200 \end{bmatrix} \tag{41}$$

and $\mathbf{D}(\mathbf{t}) = \text{diag}(v(t_1, w_1), v(t_2, w_2), v(t_3, w_3))$, with

$$v(a,b) = \begin{cases} \frac{1}{3}a^{-\frac{1}{3}}b^{-\frac{2}{3}} & \frac{a}{b} > 0.008\,856 \\ 7.787b^{-1} & \frac{a}{b} \le 0.008\,856 \end{cases}. \tag{42}$$

The Jacobian evaluated at the white point

$$\mathbf{F}_{Lab} = \mathbf{J}_{\mathcal{F}}(\mathbf{w}) = \frac{1}{3}\mathbf{J}_0\text{diag}\big(w_1^{-1}, w_2^{-1}, w_3^{-1}\big) \tag{43}$$

is useful if instead of the local linearization of $\mathcal{F}()$ a global linear (affine) approximation is desired.

REFERENCES

[1] CIE, *Colorimetry*, CIE Publ. no. 15.2, Centr. Bureau CIE, Vienna, Austria, 1986.

[2] G. Wyszecki and W. S. Stiles, *Color Science: Concepts and Methods, Quantitative Data and Formulae*, 2nd ed. New York: Wiley, 1982.

[3] H. E. J. Neugebauer, "Quality factor for filters whose spectral transmittances are different from color mixture curves, and its application to color photography," *J. Opt. Soc. Amer.*, vol. 46, pp. 821–824, Oct. 1956.

[4] P. L. Vora and H. J. Trussell, "Measure of goodness of a set of color scanning filters," *J. Opt. Soc. Amer. A*, vol. 10, no. 7, pp. 1499–1508, 1993.

[5] H. J. Trussell, G. Sharma, P. Chen, and S. A. Rajala, "Comparison of measures of goodness of sets of color scanning filters," in *Proc. IEEE Ninth Multidimensional Signal Processing Workshop*, Belize, Mar. 1996, pp. 98–99.

[6] M. J. Vrhel and H. J. Trussell, "Filter considerations in color correction," *IEEE Trans. Image Processing*, vol. 3, pp. 147–161, Mar. 1994.

[7] M. Wolski, J. P. Allebach, C. A. Bouman, and E. Walowit, "Optimization of sensor response functions for colorimetry of reflective and emissive objects," in *Proc. SPIE: Device-Independent Color Imaging and Imaging Systems Integration*, E. Walowit, Ed., 1994, vol. 2170, pp. 209–219.

[8] M. Wolski, C. A. Bouman, J. P. Allebach, and E. Walowit, "Optimization of sensor response functions for colorimetry of reflective and emissive objects," in *Proc. IEEE Int. Conf. Image Processing '95*, pp. II323–II326.

[9] G. Sharma, H. J. Trussell, and M. J. Vrhel, "Optimal nonnegative color scanning filters," *IEEE Trans. Image Processing*, submitted for publication.

[10] M. J. Vrhel and H. J. Trussell, "Optimal color filters in the presence of noise," *IEEE Trans. Image Processing*, vol. 4, pp. 814–823, June 1995.

[11] J. E. Farrell and B. A. Wandell, "Scanner linearity," *J. Electron. Imag.*, vol. 2, pp. 225–230, July 1993.

[12] H. Haneishi, T. Hirao, A. Shimazu, and Y. Mikaye, "Colorimetric precision in scanner calibration using matrices," in *Proc. 3rd IS&T/SID Color Imaging Conf.: Color Science, Systems and Applications*, Nov. 1995, pp. 106–108.

[13] H. R. Kang, "Color scanner calibration," *J. Imaging Sci. Technol.*, vol. 36, pp. 162–170, Mar./Apr. 1992.

[14] P. C. Hung, "Colorimetric calibration for scanners and media," in *Proc. SPIE*, 1991, vol. 1448, pp. 164–174.

[15] G. Sharma, "Color scanner characterization, performance evaluation, and design," Ph.D. dissertation, North Carolina State Univ., Raleigh, Aug. 1996.

[16] G. H. Golub and C. F. Van Loan, *Matrix Computations*, 2nd ed. Baltimore, MD: The Johns Hopkins Press, 1989.

[17] J. R. Magnus and H. Neudecker, *Matrix Differential Calculus with Applications in Statistics and Econometrics*. New York: Wiley, 1988.

[18] M. Wolski, J. P. Allebach, C. A. Bouman, and E. Walowit, "Optimization of sensor response functions for colorimetry of reflective and emissive objects," *IEEE Trans. Image Processing*, vol. 5, pp. 507–517, Mar. 1996.

[19] P. Chen and H. J. Trussell, "Color filter design for multiple illuminants and detectors," in *Proc. Third IS&T/SID Color Imaging Conf.: Color Science, Systems, and Applications*, Nov. 1995, pp. 67–70.

[20] P. L. Vora, "Optimization criteria and numerical analysis in the design of color scanning filters," Ph.D. dissertation, North Carolina State Univ., Raleigh, Aug. 1993.

[21] *Proc. Conf. Standards for Electronic Imaging Systems* , San Jose, CA, 28 Feb.–1 Mar. 1991, vol. CR37 of *Critical Reviews of Optical Science and Technology*, M. Nier and M. E. Courtot, Eds. Bellingham, WA: SPIE, 1991.

[22] M. J. Vrhel, R. Gershon, and L. S. Iwan, "Measurement and analysis of object reflectance spectra," *Color Res. Appl.*, vol. 19, pp. 4–9, Feb. 1994.

[23] B. K. P. Horn, "Exact reproduction of color images," *Comput. Vis., Graphics, Image Processing*, vol. 26, pp. 135–167, 1984.

Gaurav Sharma (SM'88–M'97), for a photograph and biography, see this issue, p. 932.

H. Joel Trussell (S'75–M'76–SM'91–F'94), for a photograph and biography, see this issue, p. 899.